Response to Referee Comment #2 (RC2)

Manuscript:

Long-term hydro-sediment dynamics of the Ucayali River (Amazon Basin) revealed through combined observations, remote sensing, and SWAT-Amazon modelling

Hydrology and Earth System Sciences – egusphere-2025-4101

William Santini et al.

30 March 2026

We thank Referee #2 for a careful and constructive review of our manuscript. The comments raise important points regarding model parameterization, uncertainty quantification, and the physical interpretation of the two-fraction sediment representation. We have revised the manuscript accordingly, and we address each comment in detail below.

The referee comments are reproduced in italic, followed by our responses.

Sincerely,
W. Santini et al.

General Comments

The manuscript proposes a novel framework integrating remote sensing data with hydrological and hydraulic modelling to monitor hydro-sedimentary fluxes in the Amazon River.

The manuscript provides a clear advancement in hydro-sedimentary modelling of large rivers and it could be considered for publication on HESS after clarifications and revisions. I have listed below some points asking the Authors to address them to improve the current manuscript.

Major comments

1. Line 123/132. The Authors have considered two groups of sediments: fine sediments (10-20 μm, fine and medium silt) and sands (80-120 μm, very fine sands). What is the potential effect in model accuracy of having neglected the material with an intermediate diameter?

We thank the reviewer for this relevant comment.

In the present framework, the two sediment classes should be understood as a simplified representation of a continuous particle-size distribution that is predominantly bimodal in Amazonian white rivers, with a fine mode (silts and clays) and a very fine sand mode (Fig RC2.1). The reported diameter ranges (10–20 µm and 80–120 µm) therefore correspond to mean values of these dominant groups rather than strict granulometric bounds.

As a result, intermediate particle sizes (e.g. coarse silts in the 20–63 µm range) are not neglected, but are implicitly included within these two fractions depending on their physical behaviour. Coarse silts may either behave as wash-load when transported as aggregates or cohesive particles, or close to graded suspension when non-cohesive. Given the typical hydraulic conditions of large Amazonian rivers, their Rouse numbers remain low, so that they predominantly behave as fully suspended material and contribute only marginally to uncertainty arising from the two-fraction representation.

In the transport capacity equations, this representation relies on a single mean diameter for the sand fraction. Therefore, accounting for intermediate particle sizes is simply equivalent to perturbing this representative diameter. This effect has already been explored through the Sobol sensitivity analysis and uncertainty propagation, which show that its influence on sediment budget indicators remains limited (on the order of a few percent to ~10% when combined with other parameters). Overall, the omission of an explicit intermediate class is not expected to significantly affect model accuracy, while avoiding an unnecessary increase in model complexity and parameter uncertainty.

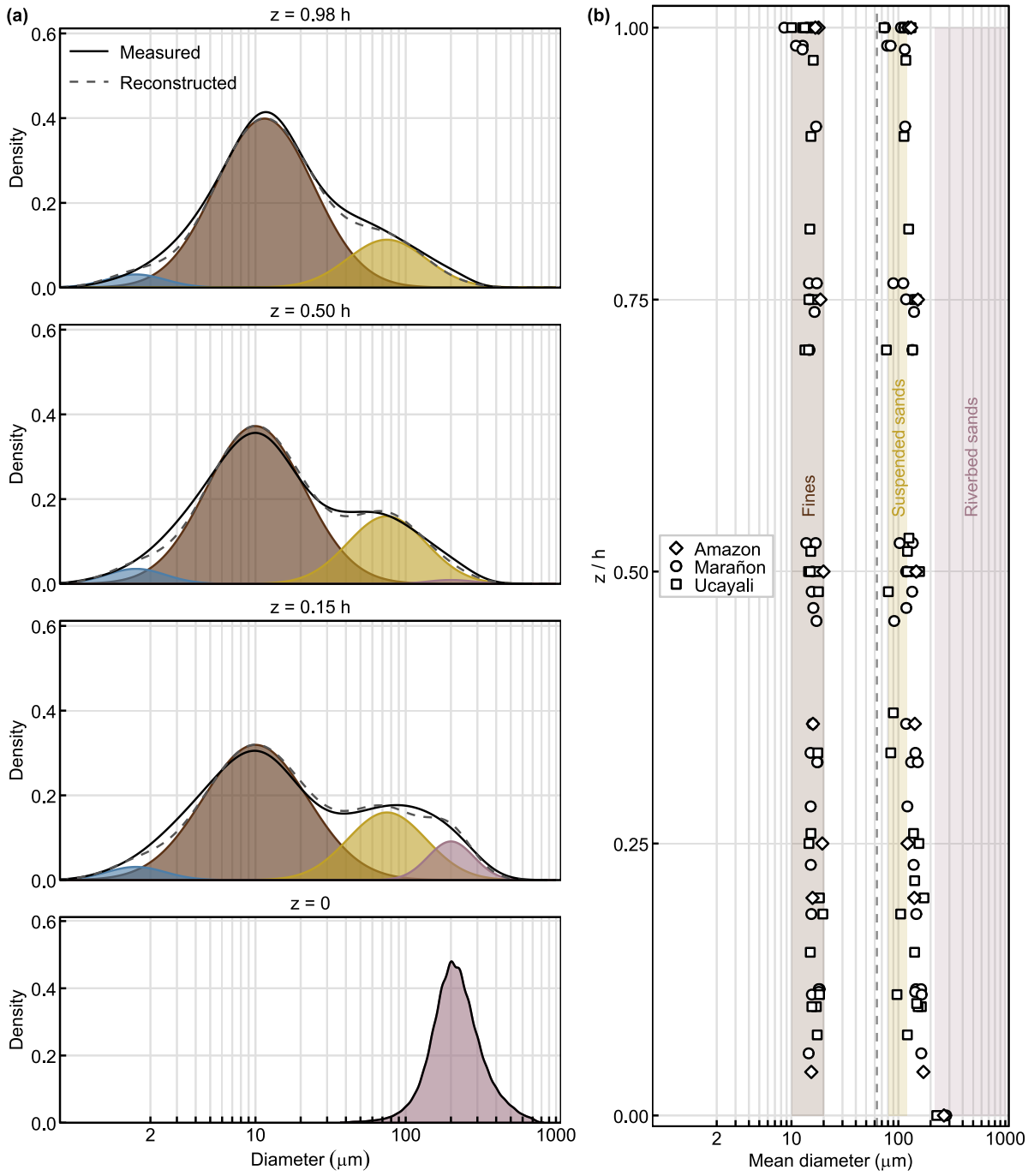

Figure RC2.1: Typical PSD of large white-water rivers in the Amazon Basin (adapted from Santini et al., 2019). (a) Particle-size distributions (PSD) measured in suspension at different relative depths and in the riverbed (Requena station, Ucayali River, 16 March 2015). The grey line shows the measured distribution, while the dashed line represents a reconstructed PSD obtained from a mixture of log-normal components corresponding to clay, silt, and sand fractions. (b) Vertical profiles of representative grain diameters for the fine and sand fractions. Symbols correspond to measurements at different stations. The dashed vertical line indicates the conventional 63 μm boundary between silt and sand.

We have added the following paragraph in Section 2 to clarify this point:

These ranges of mean diameter should be understood as representative values of the dominant PSD modes, rather than strict granulometric bounds. Intermediate particle sizes (e.g. coarse silts in the 20–63 µm range) are not neglected but are included within the fine sediment fraction defined by the 63 µm threshold used in the HyBAm monitoring protocol. Depending on their physical properties, coarse silts may either behave as wash load (e.g. aggregates) or exhibit transport dynamics closer to those of very fine sands when non-cohesive. This supports a first-order bimodal representation of suspended sediment transport at the basin scale, consistent with PSD measurements and vertical grain-size profiles presented in the Supplementary Material (Fig. S1).

Additional details have been added in the Supplementary Material.

---

2. Line 172. The Authors mentioned "two radiometric calibration-validation campaigns" for fine sediment concentration. My understanding is that the first campaign (November 2011) was for calibration and the second campaign (February 2017) was for validation. I suggest to better clarify this in the text. Furthermore, the Authors should short discuss about the extendibility to the Ucayali Basin of the data collected in few locations.

We thank the reviewer for pointing out this ambiguity. The wording in the manuscript was indeed misleading. The two campaigns were not used as independent calibration and validation datasets; rather, both campaigns contributed to the establishment of the radiometric relationship between reflectance and fine suspended sediment concentration. The text has been clarified accordingly.

We also added a short clarification regarding the applicability of the relationship across the Ucayali Basin.

The manuscript was revised as follows (section 3.3.2):

Two radiometric calibration-validation campaigns […] -> Two radiometric field campaigns […]

[…]

Relying on this dataset, a unique model for the Ucayali Basin was fitted between fine sediment concentration at the water surface and the ratio of radiometer reflectance in the NIR (841–876 nm, according to the satellite sensor bands) and red bands (620–670 nm) (see Section 5.4). This single relationship is considered applicable along the mainstem of the Ucayali River in the lowland plain because surface reflectance is largely controlled by fine silts of Andean origin, whose grain-size characteristics and optical properties are relatively homogeneous along the river continuum

(Martinez et al., 2015; Santini, 2020). In addition, the use of spectral band ratios (NIR/RED), commonly applied to reduce the influence of these potential variations in optical conditions (Doxoran et al., 2002; Martinez et al., 2015; Pinet, 2017), supports the applicability of this relationship at the basin scale considered in this study.

Figure 7 was also modified:

Calibration – validation with field radiometers -> Calibration with field radiometers

---

3. Section 3.3.3. The Authors should provide more details about this important point. Have any field measurements been made? In which sections of the basin? Have the cross-sectional variations in sediment concentration along the vertical been considered?

We thank the reviewer for this comment. Field measurements of vertical concentration profiles of fine and sand suspended sediments have been collected at several stations of the HyBAm observatory across the Amazon Basin, including the Ucayali River. In particular, 73 field measurements were conducted at Requena (44), Lagarto (28), and Pucallpa (1) using a point-sampling method to characterize vertical concentration gradients. Details on the HyBAm dataset and methodology are provided in Santini et al. (2019) and Santini (2020) and in the Supplementary Material (Section S6).

The estimation of α_f relies on the models proposed by Santini et al. (2019), which use Rouse-type formulations constrained by these observed concentration profiles to describe the vertical distribution of suspended sediments as a function of hydraulic conditions. These models were applied using hydraulic variables simulated by SWAT-Amazon to estimate α_f along the river network. Further details on the formulation and validation of the approach are provided in Santini et al. (2019).

The manuscript was revised as follows (section 3.3.3):

Due to the considerable depth of Amazonian rivers and the vertical sediment concentration gradient near the surface, the ratio α_f, relating the channel mean concentration to the surface index concentration retrieved by satellite, ranges from 1 to 1.8 according to the CZO HyBAm database (1.1–1.2 in the Ucayali). These values are derived from field measurements of vertical suspended sediment concentration profiles collected at several stations of the HyBAm observatory across the Amazon Basin, including the Ucayali River (e.g. Santini et al., 2019; Santini, 2020). To estimate α_f along the river network, the models proposed by Santini et al. (2019) were applied. These models use Rouse-type formulations constrained by observed concentration profiles to describe the vertical distribution of suspended sediments as a function of hydraulic conditions.

They were parameterized using hydraulic variables simulated by SWAT-Amazon. Further details on the formulation, validation, and field measurement protocols are provided in Santini et al. (2019) and in the Supplementary Material (Section S2).

Additional details have been added in the Supplementary Material (S2).

---

4. Section 4.1. It is unclear if (and how) morphological adjustements of channel cross-section over the simulation period were considered.

We agree that freely meandering rivers are morphodynamically active and that lateral migration of meanders can locally modify channel geometry. Reported lateral migration rates in large Amazonian rivers commonly reach several tens of meters per year, with local maxima exceeding 100 m yr^{-1} in some reaches (Abad et al., 2012; 2013; Quintana-Cobo et al., 2015). If model calibration relied on a single, morphologically active cross-section, such changes could potentially affect the stability of stage–discharge relationships.

However, morphological adjustments were not explicitly simulated in the present modelling framework. In SWAT-Amazon, the channel geometry parameters represent effective, reach-averaged hydraulic geometry for very large Amazonian rivers rather than the instantaneous geometry of a single cross-section. Lateral migration in meandering rivers mainly redistributes erosion and deposition within the meander belt and does not necessarily translate into systematic changes in the effective hydraulic control at the scale of very large reaches over decadal time scales. Furthermore, the floodplain trapping and recycling fluxes estimated in this study implicitly integrate these lateral migration processes at the reach scale, which is fully consistent with the budget framework adopted here. Consistent with this reach-scale perspective, long-term observations from the CZO HyBAm network indicate that stage-discharge relationships at the mainstem stations remain very stable over time, with no significant rating shifts. This suggests that flow conditions are primarily controlled by reach-scale channel geometry, which supports the use of time-invariant hydraulic geometry parameters over the simulation period.

The manuscript was revised as follows (section 4.1):

The main channel's trapezoidal [...]. In this framework, channel geometry parameters represent effective hydraulic conditions averaged at the reach scale rather than the instantaneous geometry of a single cross-section. Although large Amazonian rivers are morphodynamically active and may exhibit lateral migration rates of several tens of meters per year, long-term observations from the HyBAm network indicate that stage–discharge relationships remain remarkably stable over time at the mainstem stations. This suggests that flow conditions are primarily controlled by reach-scale channel geometry over the decadal time scales considered here.

5. Line 343. I would ask the Authors to shortly discuss how largely Eq.(28) is modifying Manning coefficient using the correction factor.

Eq. (28) increases flow resistance as a function of the relative water level $Y = (h - h_f)/h$ (–), which represents the stage at which water exchanges between the main channel and the floodplain begin to influence flow velocity. The parameter C_{nfp} (–) is a calibration coefficient controlling the strength of this effect when floodplain interactions occur ($Y > 0$).

In the calibrated model, C_{nfp} values along the mainstem range between 0.3 and 1. For typical flood conditions, Y varies approximately between 0 and 0.3 with a maximum value of about 0.5 during extreme floods. These extreme values ($Y = 0.5$) correspond to situations where simulated peak stages largely exceed observed values.

Under typical flood conditions, the correction remains limited to about 0–6% ($0.94 \leq \zeta_n \leq 1$) (Fig. RC2.2). Larger corrections, reaching up to about 20%, occur only in rare situations where simulated peak stages substantially exceed observations.

This range of values for the flow-resistance correction factor ζ_n is consistent with values reported in the literature for compound channel hydraulics and floodplain–channel momentum exchange (e.g. Nicollet and Uan, 1972; Smart, 1992; Shiono and Knight, 1996; Bousmar and Zech, 1999).

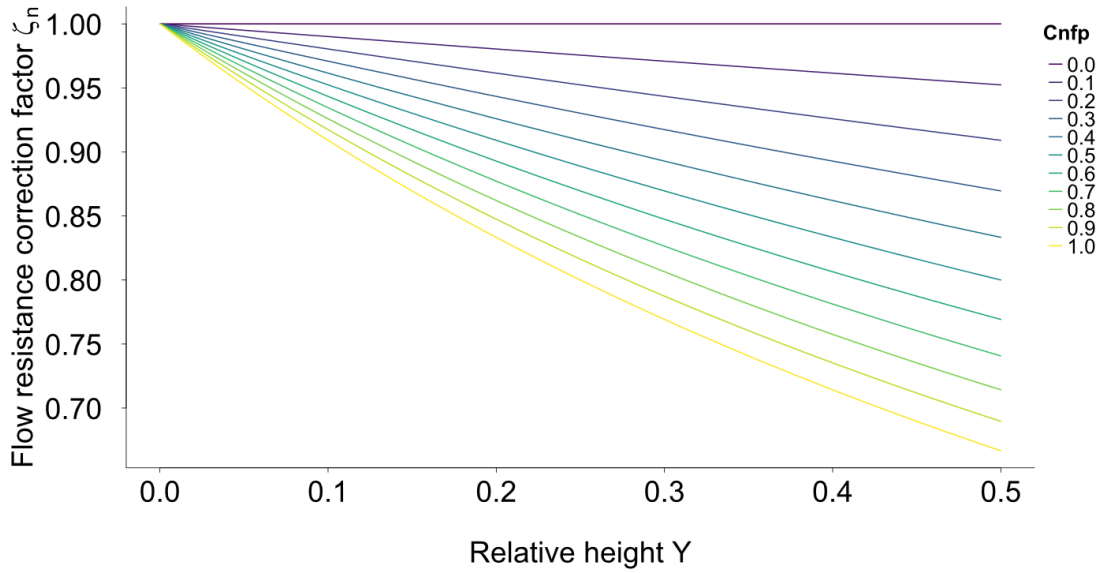

Figure RC2.2: Effect of the coefficient C_{nfp} on the Manning coefficient when the floodplain is active.

Additional details have been added in the Supplementary Material (S5).

The section 4.3.1 was revised, after Eq. (28):

In the calibrated model, C_{nfp} values along the mainstem range between 0.3 and 1. Under typical flood conditions, Y varies between 0 and about 0.3, resulting in an increase of the Manning coefficient of approximately 0–6% (see supplementary S5). Larger corrections, up to about 20%, may occur only during extreme simulated floods when Y approaches 0.5. Such variations are consistent with resistance changes reported in studies of compound channel hydraulics and floodplain–channel momentum exchange (e.g., Nicollet and Uan, 1972; Smart, 1992; Shiono and Knight, 1996; Bousmar and Zech, 1999). The coefficient C_{nfp} was calibrated during the model calibration phase to reproduce observed stage–discharge relationships at the mainstem gauging stations.

---

6. Line 364/365. I would ask the Authors to shortly provide details about the calibration of Eq.(32).

The parameters of Eq. (32), namely C_{nch} and h_{ch}, were calibrated together with the other hydraulic parameters of the routing scheme during the model calibration phase. The calibration aimed at reproducing the observed relationships between discharge or velocity and water level at the mainstem gauging stations, with particular attention to low-flow conditions where bed roughness exerts a stronger influence on flow resistance. Calibrated values of h_{ch}, range between ~ 35% and 75% of the maximum water level across the mainstem reaches, and C_{nch} between 0.12 and 0.4. The resulting correction increases the effective Manning coefficient by approximately 10–30% at low water, decreasing progressively as stage rises h_{ch} (See Fig. S7).

This behaviour is consistent with the well-known stage-dependence of bed roughness in sand-bed rivers and the two parameters remain identifiable as h_{ch} controls the threshold below which the bed roughness correction activates, reflected by an inflection in the observed stage–discharge relationship at low stage, while C_{nch} controls the amplitude of the resulting Manning coefficient increase.

The manuscript was revised as follows (section 4.3.2):

where C_{nch} (–) is a coefficient and h_{ch} (m) the water height below which the additional bed roughness correction activates. Calibrated values of h_{ch} range between 35% and 75% of the maximum simulated water level across the mainstem reaches, and C_{nch} between 0.12 and 0.4, resulting in an increase of the effective Manning coefficient of approximately 10–30% at low stage, decreasing progressively as stage rises above h_{ch} (Fig. S7). Both parameters were calibrated to reproduce the observed stage–discharge and stage–velocity relationships at the mainstem gauging stations.

7. Line 384. Yamazaki et al (2011) suggested to apply the diffusive wave equation to include backwater effect on water surface elevation. I would ask the Authors present and discuss the difference between the results from the diffusive wave and those from the kinematic wave in a Supplementary Material.

We thank the reviewer for this comment. The routing scheme implemented in the modified SWAT version used in this study already relies on the diffusive wave formulation, which was specifically selected to represent backwater effects on water surface elevation in large low-slope rivers. The limitations of the kinematic wave approximation for representing backwater effects in large rivers have been documented in the literature (e.g. Yamazaki et al., 2011).

Because the simulations presented in this study already rely on the diffusive wave formulation, a direct comparison with the kinematic wave approach was not considered necessary for the objectives of this work. Additional comparisons between routing formulations were performed during the development phase of the SWAT-Amazon framework and are documented in Santini (2020). These analyses confirmed the expected limitations of the kinematic wave approximation for representing backwater effects in large low-slope floodplain rivers.

To avoid ambiguity, the manuscript has been revised to explicitly clarify that the routing scheme used in this study is based on the diffusive wave formulation.

The manuscript was revised as follows (section 4.1.2):

SWAT-Amazon enables reach-specific selection between kinematic wave ($S_f = S_b$), suitable for steep Andean reaches, and diffusive wave approximation ($S_f = S_b + S_w$), preferred for low-slope floodplain reaches where backwater effects may occur (e.g. Yamazaki et al., 2011), with S_f (m m^{-1}) the energy gradient (or friction slope), S_b (m m^{-1}) the bed slope and S_w (m m^{-1}) the water-surface slope.

We also add the following sentence after Equation 4:

In the present study, the diffusive wave formulation was applied throughout the river network in order to account for backwater effects in the low-slope reaches of the Ucayali River.

8. Section 5.3. It seems that the model was applied (Fig.6) for the same period considered for calibration (09/2009–09/2015). The Authors should better clarify this point.

This is an important point that deserves clarification. We acknowledge that the wording in the original manuscript was ambiguous regarding the distinction between calibration and the reported performance periods, which may have given the impression that calibration and validation fully overlap. We also acknowledge that the available monitoring dataset limits the definition of a fully independent validation period for sand routing in the conventional sense. Nevertheless, model robustness is supported by: (i) consistent performance metrics over periods outside the calibration window (Table RC2.1), with reduced performance at Lagarto attributable to increased forcing and observational uncertainties rather than model degradation; and (ii) the comparison with direct gauging measurements (Fig. RC2.3), which constitute a quasi-independent validation as these observations are not explicitly used in calibration. Residual uncertainty is further addressed through the GLUE analysis presented in Section 6.

We address a complete response below:

For water routing (Section 5.1), the 2000–2016 period does not correspond to a calibration period, but rather to a common observation window used to compute performance metrics across stations, depending on data availability. Model calibration for water discharge (Table RC1.1) was conducted over the 2010–2015 period (except for Puerto Inca, for which the period was 2012–2014), selected based on data quality and availability. Furthermore, calibration does not rely on the optimization of a single time series, but on multiple hydraulic diagnostics, including water levels (Fig. 4a), velocities (Fig. 4b), and stage–discharge and stage–velocity relationships (Fig. 5). Moreover, independent hold-out periods were used to further evaluate model performance (Table RC1.1), showing consistent performance metrics across all periods.

Table RC1.1. Discharge model performance over calibration and independent validation periods. Calibration was performed over 2010–2015 (except for Puerto Inca, for which the period was 2012–2014), while independent validation periods correspond to time windows outside the calibration interval, selected based on data availability at each station. Metrics are computed using observed daily discharge records.

Station	Period type	Period	N (days)	NSE	KGE	PBIAS (%)
Lagarto	Independent validation	01/2009–12/2009	287	0.9	0.94	-1.3
Lagarto	Calibration	01/2010–12/2015	2191	0.89	0.94	-1.7
Lagarto	Independent validation	01/2016–12/2019	1162	0.84	0.90	-1.7
Puerto Inca	Calibration	09/2012–08/2014	730	0.73	0.86	-1.1
Puerto Inca	Independent validation	09/2015–08/2016	731	0.69	0.83	-7.1*
Pucallpa	Independent validation	01/2000–09/2009	3653	0.94	0.94	-4.8
Pucallpa	Calibration	01/2010–12/2015	2161	0.92	0.89	1.1
Pucallpa	Independent validation	01/2016–09/2019	1389	0.91	0.94	-1.2
Requena	Independent	01/2000–09/2009	3653	0.92	0.93	-3.8
Requena	Calibration	01/2010–12/2015	2191	0.9	0.95	0.1
Requena	Independent validation	01/2016–12/2019	1461	0.85*	0.83*	-9.5*

* Lower performance during these periods is associated with reduced quality of observed discharge data and/or precipitation inputs.

For sand routing (Section 5.3), the 09/2009–08/2015 period shown in Fig. 6 corresponds to the interval with the most reliable and dense observations, as explained in the manuscript, although data quality remains heterogeneous depending on the period and sampling protocols. This period was therefore selected for model calibration. However, outside this interval, uncertainties in sand flux observations (derived from surface sediment concentration monitoring and sediment gauging; see Supplementary Material S1) increase, which precludes the definition of a robust and fully independent validation period. In particular, at Lagarto, the NSE for the validation period decreases to 0.45 (Table RC2.1). When excluding high waters (flood peaks), the NSE remains high (0.80), indicating robust model performance under low- and intermediate-flow conditions. The lower performance is therefore mainly associated with rapid Andean flood events and related uncertainties in rainfall forcing.

Table RC2.1. Sand routing model performance over calibration and independent validation periods. Calibration was performed over 2009–2015, while independent validation periods correspond to time windows outside the calibration interval, selected based on data availability at each station. Metrics are computed using observed sand flux at surface concentration sampling time step.

Station	Period type	Period	N (days)	NSE	KGE	PBIAS (%)
Lagarto	Calibration	09/2009–08/2015	323	0.80	0.87	7.9
Lagarto	Independent validation	09/2015–08/2018	181	0.45	0.60	27.7
Requena	Calibration	09/2009–08/2015	404	0.86	0.92	-2.3
Requena	Independent validation	09/2015–08/2018	77	0.80	0.70	-24.0

Overall, reduced performance after the calibration period reflects both increased observational and forcing uncertainties rather than a degradation of model performance.

Therefore, to further evaluate model performance, we performed an additional comparison between daily simulations (discharge and suspended sand fluxes) and direct gauging measurements over the 09/2009–08/2016 period (Fig. RC2-3). This period starts with the implementation of improved sediment sampling protocols during field measurements, while simulations after 2016 were not considered due to increased uncertainties in rainfall inputs at Requena (Fig. 3d). This comparison bypasses rating curves and provides a more direct evaluation of model performance. Although not fully independent, it offers a complementary and partially independent validation, as direct gauging measurements are not explicitly used in the calibration, even though they contribute to the construction of rating curves over the full observation period. The agreement between simulations and gauging measurements supports model robustness, with bias-corrected R^2 (bR^2) values of 0.90 for discharge and 0.88 for sand fluxes (Fig. RC2-3).

The corresponding results have been added in the Supplementary Material (Fig. S9) and are briefly discussed in the revised manuscript. We have also revised the text to explicitly distinguish between calibration, performance assessment, and the different sources of observational constraints.

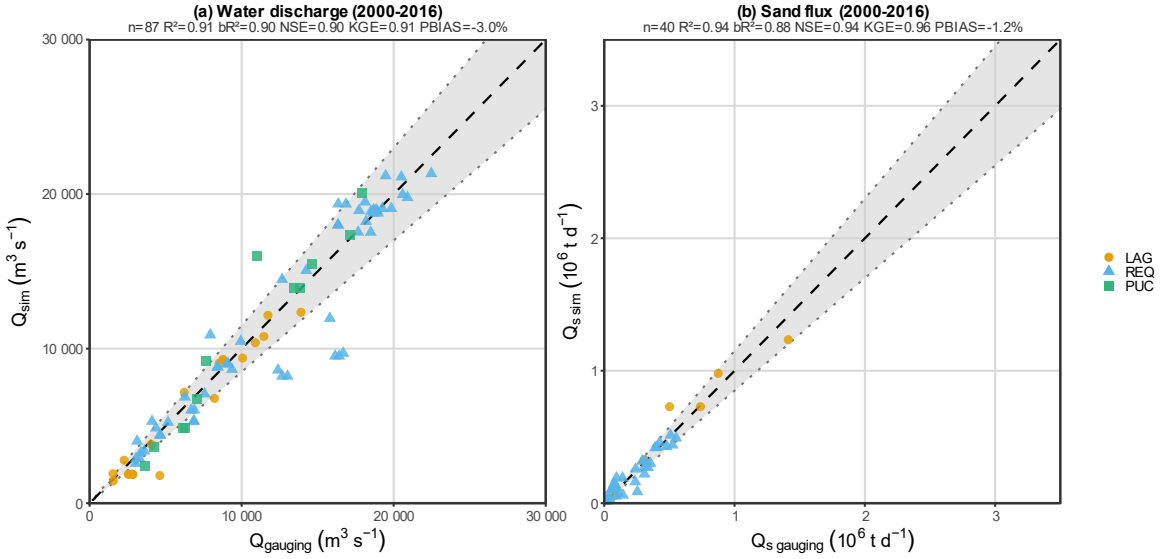

Figure RC2.3: Comparison of simulated and (a) measured river discharge and (b) suspended sediment flux at gauging stations in the Ucayali basin. Simulated values ($\boldsymbol{Q_{sim}}$, $\boldsymbol{Q_{s\ sim}}$) correspond to daily outputs from the SWAT-Amazon model extracted at the dates of field measurements. Observed values ($\boldsymbol{Q_{gauging}}$, $\boldsymbol{Q_{s\ gauging}}$) are direct field measurements, independent of rating curve derivation. The dashed line indicates the 1:1 relationship, and the shaded band represents the ±15% envelope. The Puerto Inca station was excluded, as its sub-daily flood pulse dynamics are not adequately captured at the model's daily time step. Axis ranges reflect the observed variability of $\boldsymbol{Q}$ and $\boldsymbol{Q_s}$ across all stations. Statistical indicators are computed over all stations pooled: n = number of paired observations; R^2 = coefficient of determination; bR^2 = bias-corrected coefficient of determination; NSE = Nash–Sutcliffe efficiency; KGE = Kling–Gupta efficiency; PBIAS = percent bias.

The manuscript was revised as follows:

Section 5.3

Calibration focused on the 09/2009–08/2015 period, when sediment monitoring protocols were enhanced, including higher sampling frequency at Requena between 11/2012 and 06/2013, where one sample was collected each two days plus three sampling repetitions each ten days. Beyond, sampling was conducted at five-day intervals during the wet period between July 2013 and September 2015. Additionally, the concentration gaugings were performed in all sites with a higher number of samples collected throughout the cross-section, particularly in the first half of the water column, to ensure more accurate sand concentration calculations. Outside this interval, uncertainties in sand flux observations increase, which complicates the definition of a robust and fully independent validation period (see Supplementary Material S9 for a summary of model performance across periods). The lower performance outside the calibration period primarily reflects uncertainties in rainfall forcing and observations, particularly during rapid Andean flood events, rather than a degradation of model performance. To further evaluate model performance, direct comparisons between simulations and gauging measurements were performed (Supplementary Material, Fig. S9). These complementary evaluations support the temporal robustness of the model despite observational limitations and data heterogeneity.

Supporting analyses and details are now provided in the Supplementary Material (S9).

Minor comments

9. Line 135. The quality of Fig.1 should be improved.

Thank you for this comment. The lower quality of Fig. 1 results from the resolution used in the EGUsphere discussion paper. The figure is already provided at full resolution (300 dpi) and will appear in high quality in the final manuscript.

10. Line 325. On compound channels hydrodynamics see also: Proust, S., & Nikora, V. (2020). Compound open-channel flows: effects of transverse currents on the flow structure. Journal of Fluid Mechanics, 885, A24. https://doi.org/10.1017/jfm.2019.973

Thank you for this suggestion. The reference has been added in the revised manuscript (section 4.3.1) to complement the discussion on compound channel hydrodynamics.

11. Line 342. How was the coefficient Cfnp calibrated ?

The coefficient C_{nfp} was calibrated together with the other hydraulic parameters of the routing scheme during the model calibration phase. The calibration aimed at reproducing the observed relationships between discharge and water level at the mainstem gauging stations. The resulting values range between 0.3 and 1 along the mainstem, reflecting spatial variations in floodplain interaction intensity. This clarification has been added in Section 4.3.1 of the revised manuscript (see response to Referee Comment #5).

12. Line 667/668. I suggest to further elaborate the discussion on the Kbed coefficient of erosion susceptibility. You might provide details on that at line 289.

We thank the reviewer for this suggestion. A short clarification has been added in Section 4.2.4 (line ~289) to explain the role of the coefficient K_{bed} , which represents the susceptibility of the riverbed to erosion when the simulated sand transport capacity exceeds the available sand load. This parameter therefore controls the potential entrainment of bed material into suspension and regulates the contribution of riverbed erosion to the simulated suspended sand flux. It was calibrated together with the other sediment routing parameters during the model calibration phase.

Proposed revision in the manuscript:

(i) Section 4.2.3, after Eq. 18:

where K_{bed} (–) is a coefficient ($0 \leq K_{bed} \leq 1$) representing the susceptibility of the channel bed to erosion when the simulated sand transport capacity exceeds the available sand load. This parameter governs the potential entrainment of bed material into suspension and thus the possible contribution of riverbed erosion to the simulated suspended sand flux.

(ii) Section 6.3:

Lastly, the distinction between E_{bk} and E_{bed} is partly supported by the calibration experiments. When bed erosion is activated ($k_{bed} > 0$), the model tends to generate rapid and abrupt peaks in simulated sand flux once the transport capacity exceeds the available sand load, whereas adjusting C_{bk} produces a smoother and more progressive increase in sand concentration that better reproduces the secondary peaks observed during the recession phase. The calibrated values of K_{bed} remain very small ($K_{bed} \ll 1$), suggesting that riverbed erosion contributes only weakly to the simulated suspended sand flux in the main stem, although a minor contribution cannot be fully excluded.

---

13. Line 785. List of model parameters. Water kinematic viscosity has two different symbols.

Thank you for pointing out this inconsistency. The notation of the water kinematic viscosity has been corrected to ensure a consistent symbol throughout the manuscript and in the list of model parameters.

Additional references

Bousmar, D. and Zech, Y.: Momentum transfer for practical flow computation in compound channels, Journal of Hydraulic Engineering, 125, 696–706, https://doi.org/10.1061/(ASCE)0733-9429(1999)125:7(696), 1999.

Doxaran, D., Froidefond, J. M., Lavender, S., and Castaing, P.: Spectral signature of highly turbid waters: Application with SPOT data to quantify suspended particulate matter concentrations, Remote Sensing of Environment, 81, 149–161, https://doi.org/10.1016/S0034-4257(01)00341-8, 2002.

Shiono, K. and Knight, D. W.: Turbulent open-channel flows with variable depth across the channel, Journal of Fluid Mechanics, 222, 617–646, https://doi.org/10.1017/S0022112091001246, 1991.